Numerical Simulation Of A Pollutant Transport In Lower Atmosphere Layer From Thermal Power Plants

ALIBEK ISSAKHOV, AIYMZHAN BAITUREYEVA
Department of Mechanics and Mathematics
al-Farabi Kazakh National University
Al-Farabi ave., 71, Almaty, 050040
REPUBLIC OF KAZAKHSTAN
alibek.issakhov@gmail.com, abaitur@yandex.kz
http://www.kaznu.kz

Abstract: The purpose of this work is to investigate the distribution of pollutions in the atmosphere. The fast development of the industry leads to an increase in the number of factories, plants, thermal power plants, nuclear power plants, that is why there are increasing the amount of emissions into the atmosphere. It is harmful to human health and the environment. That is why it is very important to control emissions, to keep them at a safe level for the environment. The best way to assess is the creating of the mathematical model of the gaseous substances motion. Such model includes various physical, chemical and weather factors. In the present paper is considered a model problem, which allows to validate the correctness of the chosen mathematical models and numerical solution algorithm. The model takes into account the physical parameters of the materials, allows to calculate the chemical reaction between the reactants and the distribution of mass fractions of emission depending on t he wind velocity. The calculations were performed using the ANSYS Fluent software package. In the end there are given results of numerical solutions and the graphs. This task allows to test the existing mathematical model in order to create in the further more accurate three-dimensional model of the emissions distribution in the atmosphere. Ekibastuz State District Power Plant 2 was chosen as an actual physical model. It located in Ekibastuz, Kazakhstan.

Key-Words: Navier-Stokes equations, mass transfer, numerical simulation, air pollution, concentration, power plants.

1 Introduction

Air pollution from year to year is becoming more global and serious issue of global importance. Continuous development and population growth in urban areas, a number of problems related to the environment, such as deforestation, emission of toxic materials, solid waste emissions, air pollution and more, attracts more attention than ever before. The industry develops all over the world, resulting in a growing number of factories, thermal power plants, nuclear power plants, which produce large amounts of pollutants. Emissions lead to different environmental problems, which are harmful to human health and the environment. The problem of air pollution in cities has become so serious that there is a need for timely information about changes in the level of contamination [1–3]. In addition to the emission of pollutants from flue pipe in the process of thermal power plants work there is produced slag waste. Also it has a detrimental effect on the cooling ponds. Increasing of water temperature has an impact on t he change of flora and fauna.

Millions tons of gaseous sulfur and nitrogen oxides are emitted into the environment each year. The share of thermal power plants in anthropogenic emissions of these oxides is 45-65% and 15-45%, respectively [4]. Further development of the thermal energy is highly dependent on ensuring an acceptable level of power plants impact on the environment and their safety for the ecology [1]. Getting into the atmosphere, the gaseous emissions are distributed in the air, react chemically, and fall in the form of dry and liquid precipitation on t he surrounding surface of the earth (plants, soil, water, buildings, etc.). Depending on various physical, chemical and weather factors, contaminants can reach the surface of the earth at a distance of 500-1000 km from the source. This distance increases with the source capacity [4–6].

The study of this process in Kazakhstan is especially important. Kazakhstan has large reserves of energy

resources (oil, gas, coal, uranium) and is a raw country living through the sale of natural energy reserves (80% of exports - raw materials and industrial export share is decreasing annually). According to statistics, Kazakhstan's energy consists by almost 87% coal, and by 2020 the proportion of hard fuel will be 66% of the total volume in the generation of emissions. Thus, the energy sector is a major polluter of the air basin of Kazakhstan.

To simulate such large-scale problems, it is necessary to solve the model problem to validate the selected mathematical model and numerical algorithm. For this purpose, in this paper we investigate the motion of substance coming out of the pipe perpendicular to the main flow in the channel. Input conditions for exit from the pipe and the crossflow velocity described by the different profiles. The speed ratio is expressed through $R = \frac{U_{jet}}{U_{crossflow}} = 1{,}5$. In this paper there are compared the results for different velocity profiles and their influence on the further movement the substances. Substance B, emerging from the pipe, reacts with the substance of the main flow A, thereby forming C. There have been studied concentrations of each of them. The substances are selected with the purpose that the Damköhler number is 1. The flow is incompressible. The calculations were performed using the software package ANSYS Fluent. A similar study was conducted by the foreign researchers [8, 9] and the aim of this study was to compare the obtained data with the previous results.

2 Two-dimensional problem

2.1 Scheme and dimensions of the computational domain

The following Figure 1 shows the scheme and the dimensions of the computational domain. Substance A enters through the left edge of “inlet 1”, a substance B across the tube input “inlet 2”, the output is in the right border – “outlet”. The grid of the main part of the channel has 640x160 elements, the grid of the pipe: 40x80 elements. As a result, the number of elements was 106 481. F or the calculations, which carried out at ANSYS, all values were set in meters, geometry was built in ANSYS Geometry. Software grid for calculations by the TFS MCM has been built by using Pointwise program. Viscosity Laminar method has been applied for solving equations in ANSYS Fluent. For calculating the concentration of the spread there has been applied Species Transport. Discretization of equations was carried out with the help of SIMPLE method. Convergence condition was set as $\varepsilon = 0.00001$.

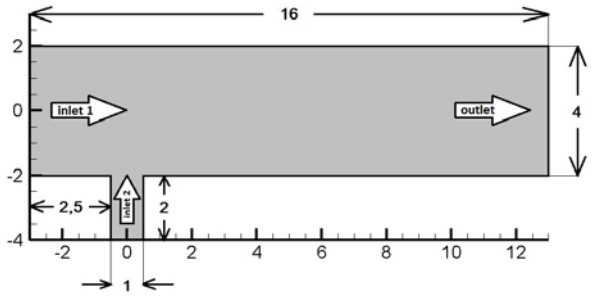

Fig.1 – Diagram of the computational domain.

2.2 Mathematical model

A detailed review of recent works about a flow from jet in crossflow can be found in [10]. Previous authors have investigated numerically the velocity field [11-16], and the passive scalar concentration field was considered in [17-19]. Also numerical simulation of the velocity field was considered in [20-24]. Today, numerical simulation increasingly used for study of the jet flow in crossflow. In [25-26] is simulated flow from jet in crossflow with the help of Reynolds-averaged Navier-Stokes equations (RANS) and the numerical results obtained for the velocity field are compared with experimental data. In [27-29] numerical simulation is carried out using the method of large eddy simulation (LES), which gives much better results than the RANS approach. In [30, 31] obtained a good coherence of average velocities and turbulence intensity of the experimental results with those obtained by direct numerical simulation (DNS) [18, 32]. The foundation for the process numerical simulation of the mathematical model formed by the Navier-Stokes equations consisting of the equation of continuity and the equations of motion.

$$\frac{\partial u}{\partial x} + \frac{\partial w}{\partial z} = 0 \tag{1}$$

$$\rho\left(u\frac{\partial u}{\partial x} + w\frac{\partial u}{\partial z}\right) = -\frac{\partial p}{\partial x} + \mu\left(\frac{\partial^2 u}{\partial x^2} + \frac{\partial^2 u}{\partial z^2}\right) \tag{2}$$

$$\rho\left(u\frac{\partial w}{\partial x} + w\frac{\partial w}{\partial z}\right) = -\frac{\partial p}{\partial z} + \mu\left(\frac{\partial^2 w}{\partial x^2} + \frac{\partial^2 w}{\partial z^2}\right) \tag{3}$$

The continuity equations for Y_A and Y_B components were used to calculate the concentration.

$$\rho\left(u\frac{\partial Y_A}{\partial x}+w\frac{\partial Y_A}{\partial z}\right)=\rho\Gamma_A\left(\frac{\partial^2 Y_A}{\partial x^2}+\frac{\partial^2 Y_A}{\partial z^2}\right)-k_1 Y_A Y_B \quad (4)$$

$$\rho\left(u\frac{\partial Y_B}{\partial x}+w\frac{\partial Y_B}{\partial z}\right)=\rho\Gamma_B\left(\frac{\partial^2 Y_B}{\partial x^2}+\frac{\partial^2 Y_B}{\partial z^2}\right)-k_2 Y_A Y_B \quad (5)$$

According to Dalton's law

$$Y_C=1-Y_A-Y_B \quad (6)$$

Here, $u, w-$are the components of the velocity, $\rho-$density, $\mu-$dynamic viscosity, $\Gamma_A,\ \Gamma_B-$diffusion coefficients, $k_1,\ k_2-$ reaction rate constants.

2.3 Boundary and initial conditions

Boundary conditions were set as follows: for the inlet 1 and inlet 2 - 'Velocity-inlet', for the outlet - 'Pressure-outlet', for the walls - 'Wall'.

Initial conditions:

For entry of the main channel inlet 1 different versions of the velocity profile u were considered:

$$u1:\quad u=u^* \quad (7)$$

$$u2:\quad u=u^*\left(1-e^{-4.5\left(1-\frac{r^2}{4}\right)}\right),\quad r=y \quad (8)$$

$$u3:\quad u=u^*\left(1-e^{-5\left(1-\frac{r^2}{4}\right)}\right),\quad r=y \quad (9)$$

$$u4:\quad u=u^*\left(1-e^{-5.5\left(1-\frac{r^2}{4}\right)}\right),\quad r=y \quad (10)$$

Other parameters were set as constant: $w=0$, $Y_A=1, Y_B=0$.

For the pipe entry inlet 2: $u=0, w=2Ru^*\left(1-4l^2\right),\ \ l=x,\ Y_A=0, Y_B=1$.

Here u^* varies depending on the selected material. For substance A and B was set the oxygen O_2. To obtain the required Reynolds number $\mathrm{Re}=\frac{\rho u_{crossflow} D}{\mu}=25$ and taking into account the fact that dynamic viscosity of the oxygen is $\mu=1{,}919\text{e-}05\ \mathrm{kg\cdot m^2/s}$, the density $\rho=1{,}299874\ \mathrm{kg/m^3}$, the velocity $u^*=0{,}000369074233\ \mathrm{m/s}$. The hydraulic diameter $D=1m$. In order to Schmidt number was equal to one, the diffusion coefficient was defined as the number $0{,}67737051\,\mathrm{m^2/s}$.

In ANSYS Fluent all calculations are made in real size, so in the present case the actual parameters have been specified. In the calculations by the TFS MCM there were used dimensionless parameters.

Table 1 - The boundary conditions

Parameters	inlet 1	inlet 2	wall	outlet
u	See (7) – (10)	$u=0$	$u=0$	$\frac{\partial u}{\partial x}=0$
w	$w=0$	See (12)	$w=0$	$\frac{\partial w}{\partial x}=0$
p	Eq. (2)	$p=p_{atmo}$	Eq. (3)	Eq. (2)
Y_A	$Y_A=1$	$Y_A=0$	$\frac{\partial Y_A}{\partial x}=0$	$\frac{\partial Y_A}{\partial x}=0$
Y_B	$Y_B=0$	$Y_B=1$	$\frac{\partial Y_B}{\partial x}=0$	$\frac{\partial Y_B}{\partial x}=0$
Y_C	$Y_C=0$	$Y_C=0$	$\frac{\partial Y_C}{\partial x}=0$	$\frac{\partial Y_C}{\partial x}=0$

For a discretization of the system (1) - (6) is used the control volume method. For this we represent the Navier - Stokes equation for the concentration in

the form of integral conservation laws for an arbitrary fixed volume Ω with boundary dΩ [33, 34]:

$$\int_{\Omega}\left(\frac{\partial U}{\partial t}+\frac{\partial F_i}{\partial x_i}+\frac{\partial G_i}{\partial x_i}-B_i\right)\partial\Omega=0 \qquad (11)$$

Where

$$U=\begin{pmatrix}0\\u_j\\C\end{pmatrix},\ F_i=\begin{pmatrix}u_i\\u_iu_j+p\delta_{ij}-\tau_{ij}\\u_jC\end{pmatrix},$$

$$G_i=\begin{pmatrix}0\\\nu\dfrac{\partial u_i}{\partial x_j}\\\chi\dfrac{\partial C}{\partial x_j}\end{pmatrix},\ B=\begin{pmatrix}0\\0\\0\end{pmatrix}$$

The equations (11) can be written in the form

$$\int_{\Omega}\left(\frac{\partial U}{\partial t}-B\right)d\Omega+\oint_{\partial\Omega}\left(F_i+G_i\right)n_i d\Gamma=0 \quad (12)$$

represent the equations (12) to the following form

$$\oint_{\Omega}\left(\frac{\partial U}{\partial t}\right)d\Omega+\oint_{\partial\Omega}\left(F_i+G_i\right)n_i d\Gamma=\int_{\Omega}B_i d\Omega \quad (13)$$

Grid functions will be defined in the center of the cell, and the values of flows across the border in divided cells. The volume of the cell is denoted by grid functions.

Now we perform discretization of the equation (13) by the control volume (CV) and the control surface (the CS)

$$\sum_{CV}\left(\frac{\Delta U}{\Delta t}\right)\Delta\Omega+\sum_{CS}\left(F_i+G_i\right)n_i\Delta\Gamma=\overline{B}_i\Delta\Omega \qquad (14)$$

or it is possible to write equation (14) in the form:

$$\sum_{CV}\Delta U\Delta\Omega+\sum_{CS}\Delta t\left(F_i+G_i\right)n_i\Delta\Gamma=\Delta t\,\overline{B}_i\Delta\Omega \qquad (15)$$

2.4 Numerical simulation

For the numerical solution of equations (1) - (6) is used splitting scheme by physical parameters [33-35]. For the numerical implementation of the system (1) - (6), is used the discretization of the type (15). At the first stage it is assumed that the transfer of momentum carried out only by convection and diffusion. The intermediate velocity field is found by 5-step Runge - Kutta method [36, 37]. At the second stage the pressure field is found based on the intermediate velocity field. Poisson equation for the pressure field is solved by Jacobi method. In a third step it is assumed that the transfer is carried out only by the pressure gradient. At the fourth step, as well as the equations of motion, 5-step Runge - Kutta method numerical solution was used to solve equation for a passive impurity. For solving the equation of the concentration is also used finite volume method and the same calculations as for the equations of motion [36, 37]. The problem algorithm is parallelized on high-performance systems. The calculations were performed on cluster systems URSA and T-Cluster by Research Institute of Mathematics and Mechanics at the Kazakh National University named after al-Farabi.

Mathematical numerical algorithm looks like this:

I) $$\int_{\Omega}\frac{\vec{u}^{*}-\vec{u}^{n}}{\tau}d\Omega=-\oint_{\partial\Omega}\left(\nabla\left(\vec{u}^{n}\vec{u}^{*}-\tau_{ij}\right)-\nu\Delta\vec{u}^{*}\right)n_i d\Gamma$$

II) $$\oint_{\partial\Omega}\left(\Delta p\right)d\Gamma=\int_{\Omega}\frac{\nabla\vec{u}^{*}}{\tau}d\Omega$$

III) $$\frac{\vec{u}^{n+1}-\vec{u}^{*}}{\tau}=-\nabla p$$

IV) $$\int_{\Omega}\frac{C^{*}-C^{n}}{\tau}d\Omega=-\oint_{\partial\Omega}\left(\nabla\vec{u}^{n}C^{*}-\chi\Delta C^{*}\right)n_i d\Gamma$$

2.5 Numerical results

Next, the results of calculations and comparative analysis of the following parameters are presented : the velocity, concentration and temperature fields.

Velocity

The Figure 2 shows the results for the horizontal and vertical profile of the velocity at the initial velocity profile $u3$ for the main channel.

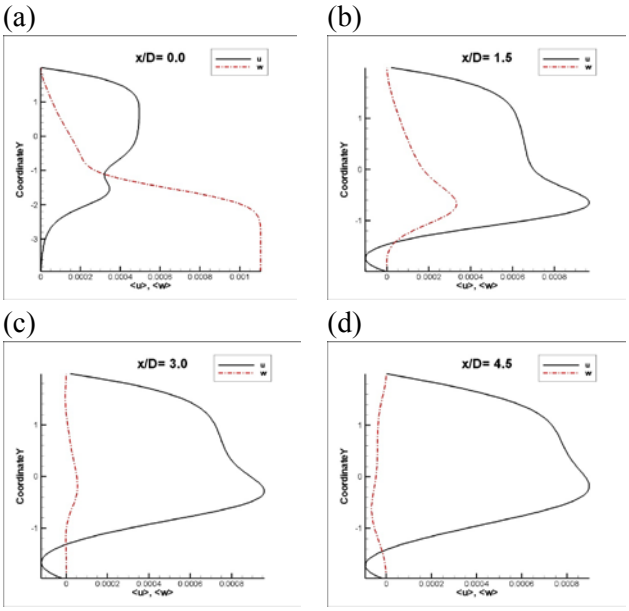

Fig.2 – The profiles of vertical and horizontal velocity components: (a) x / D = 0.0, (b) x/D = 1.5, (c) x/D = 3.0, (d) x/D = 4.5 [m].

Below are the velocity profiles u for different initial velocities at different distances.

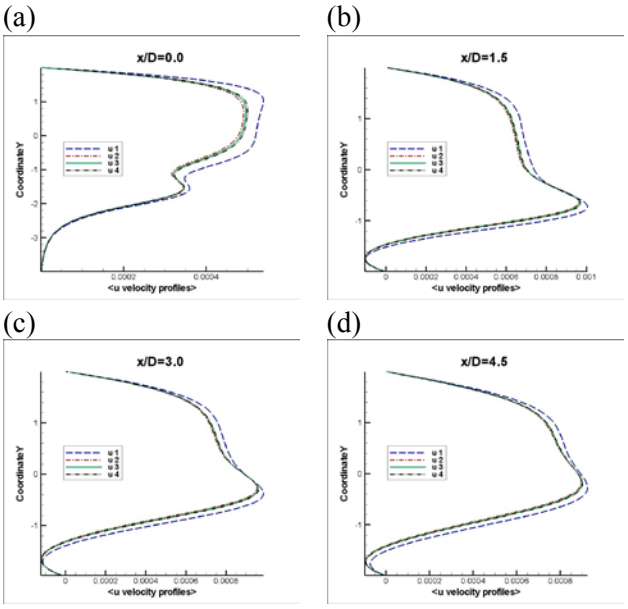

Fig.3 – Comparison of velocity profiles at different distances (a) x/D = 0.0, (b) x/D = 1.5, (c) x/D = 3.0, (d) x/D = 4.5 [m]

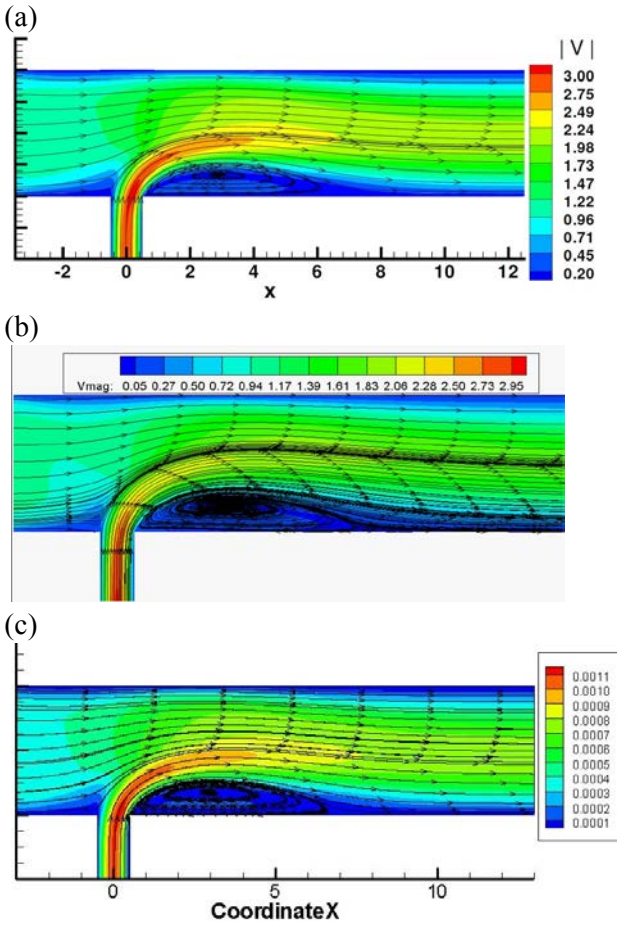

Fig.4 – The contour of velocity and streamlines: (A) the results of Denev and etc.; (B) the results obtained by calculations on T FS MCM software; (C) the results obtained by ANSYS.

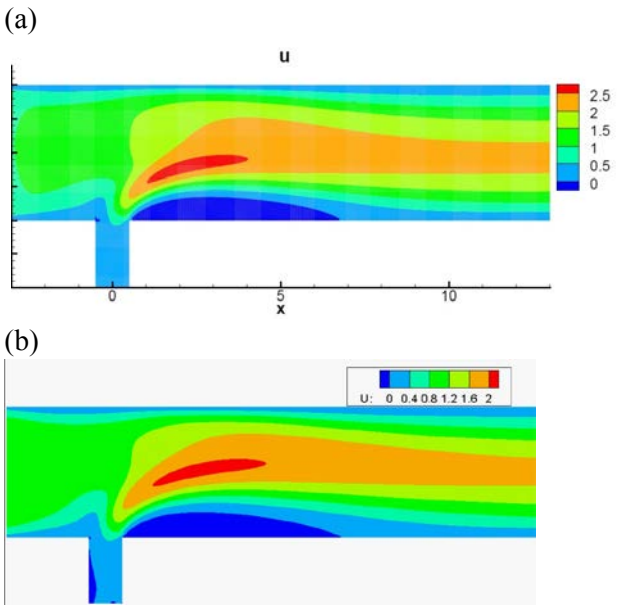

(c)

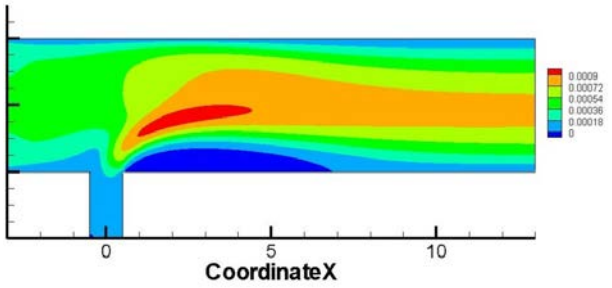

Fig.5 - The contour of the u velocity component: (A) the results of Denev and etc.; (B) the results obtained by calculations on T FS MCM software; (C) the results obtained by ANSYS.

(a)

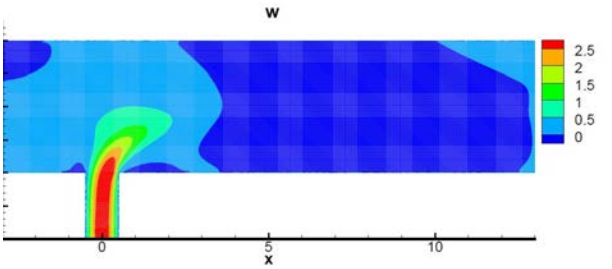

(b)

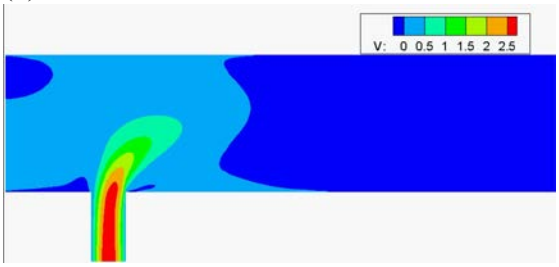

(c)

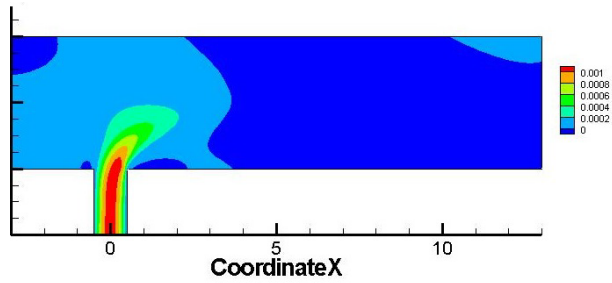

Fig.6 - The contour of the w velocity component: (A) the results of Denev and etc.; (B) the results obtained by calculations on T FS MCM software; (C) the results obtained by ANSYS.

The Figure 3 clearly shows that the difference between the profiles $u2, u3$ and $u4$ practically absent, but the profile $u1$ is very different from them. We conclude that it is important to set the velocity profile across the function, rather than through constant, since it significantly affects the result and more accurately describes the real physical processes that give as cl ose as p ossible result similar to the real nature. Figure 4 shows the flow streamlines and velocity values throughout the computational domain. Figures 5-6 illustrate the contours of u and w velocity components respectively.

Velocity values in the range of results are different due to the fact that at ANSYS actual values have been set, in the TFS MCM – dimensionless parameters.

Concentration

Figures 7, 8 and 9 illustrate the results of the concentration profile of substances A, B and of the resulting reactant C at different sections, respectively.

(a) (b)

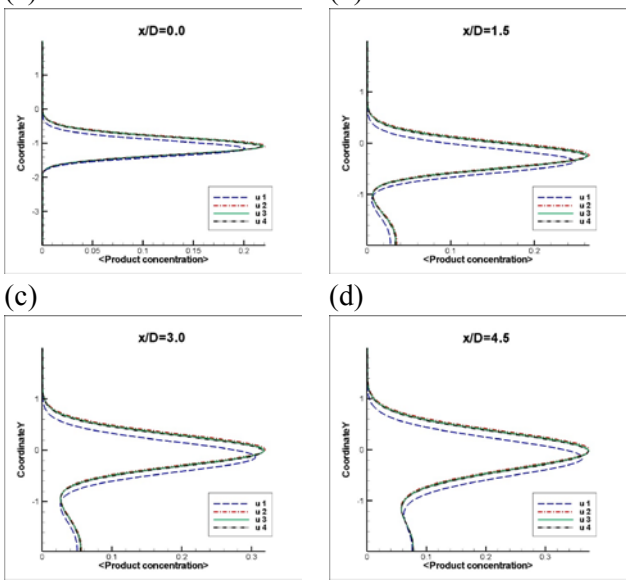

(c) (d)

Fig.7 – Profiles of concentration for the reaction product C at different distances for various initial velocity profiles: (a) x/D = 0.0, (b) x/D = 1.5, (a) x/D = 3.0, (z) x/D = 4.5 [m].

(a) (b)

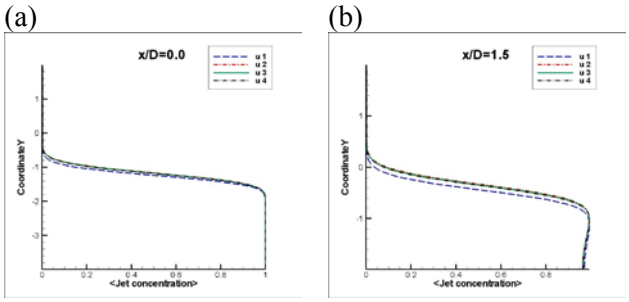

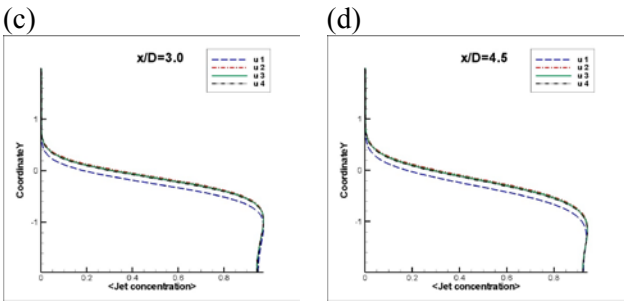

Fig.8 – The profiles of substance B concentration at different distances for different initial velocity profiles: (a) x/D = 0.0, (b) x/D = 1.5, (c) x/D = 3.0, (d) x/D = 4.5 [m].

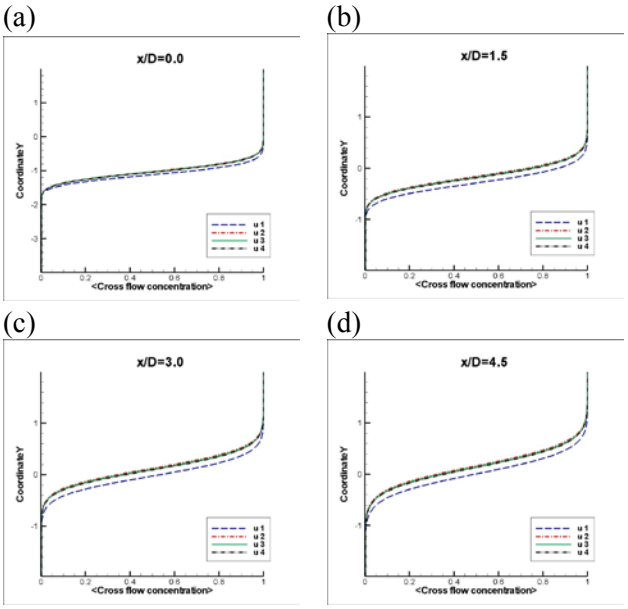

Fig.9 – The profiles of substance A concentration at different distances for different initial velocity profiles: (a) x/D = 0.0, (b) x/D = 1.5, (c) x/D = 3.0, (d) x/D = 4.5 [m].

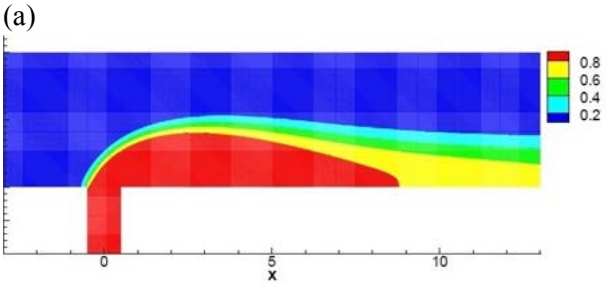

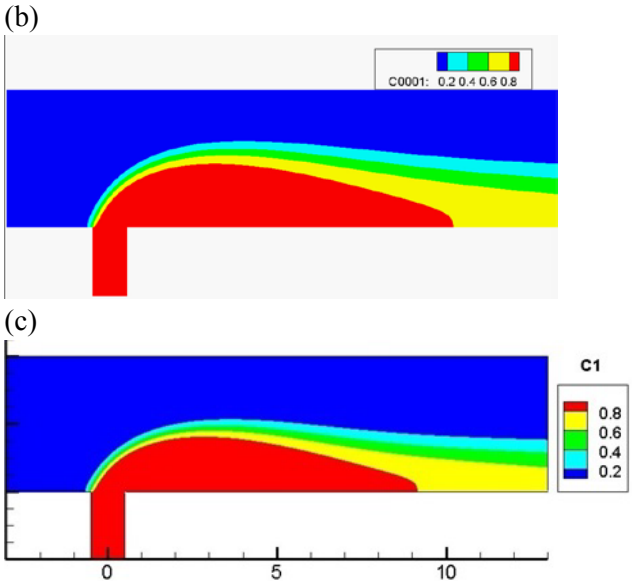

Fig.10 – Comparative analysis of the substance A distribution: (A) the results of Denev and etc.; (B) the results obtained by calculations on TFS MCM software; (C) the results obtained by ANSYS.

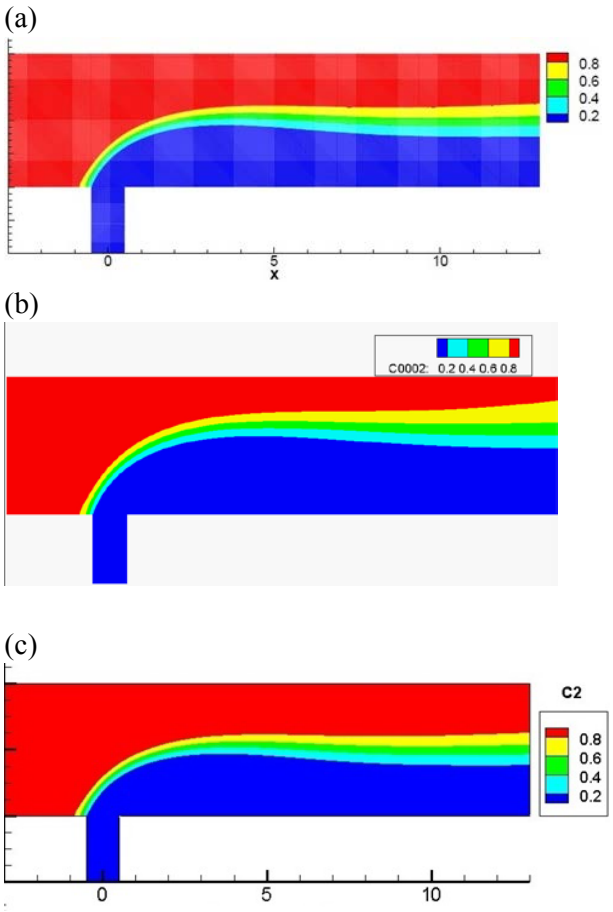

Fig.11 – Comparative analysis of the substance B distribution: (A) the results of Denev and etc.; (B)

the results obtained by calculations on TFS MCM software; (C) the results obtained by ANSYS.

(a)

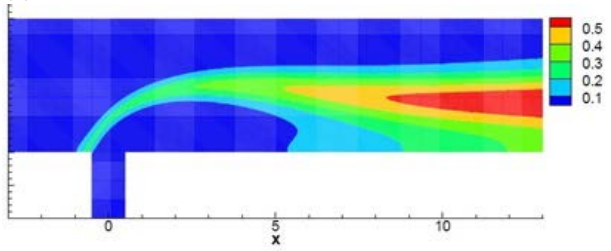

(b)

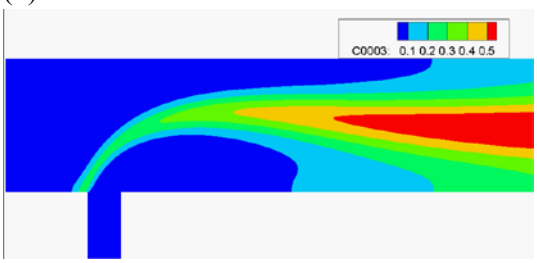

(c)

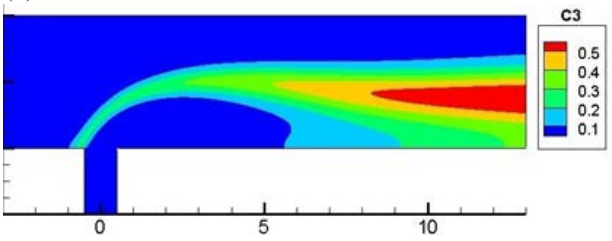

Fig.12 – Comparative analysis of the substance C distribution: (A) the results of Denev and etc.; (B) the results obtained by calculations on TFS MCM software; (C) the results obtained by ANSYS.

Figures 10-12 presents a comparative analysis of the concentrations spread obtained in the course of this work and the results obtained by foreign researchers [8, 9], where C1, C2, C3 - the concentration of substances A, B and C, respectively.

Temperature

The following Figure 13 shows the results for the temperature obtained by performing calculations on the TFS MCM and ANSYS.

(a)

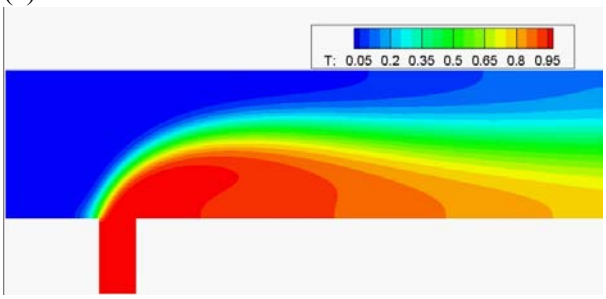

(b)

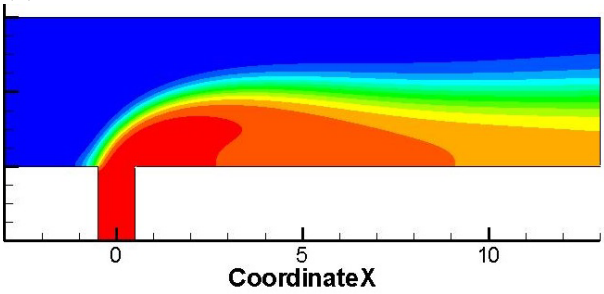

Fig.13 – Comparative analysis of the temperature field: (A) the results obtained by calculations on TFS MCM software; (B) the results obtained by ANSYS.

3 Three-Dimensional problem

3.1 Scheme and dimensions of the computational domain

Test problem is two-dimensional, in this section we consider a three-dimensional problem in two ways: in a scale of 1:1000 and 1:1. The calculations are conducted by using the program software package ANSYS Fluent 16.0. The three-dimensional box with a pipe was chosen as the computational domain. Emissions spread from the hole of the pipe and one of the walls has been set as input for the wind flow. The opposite wall was defined as an outlet. Figure 14 shows the geometry and grid of computing field. Many parameters were taken from previous studies of foreign authors [5].

(a)

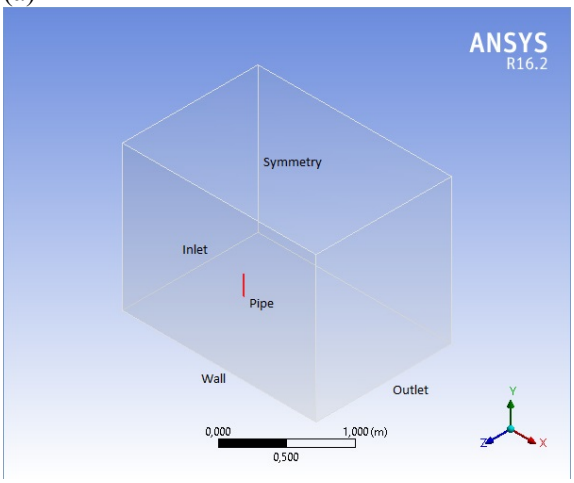

(b)

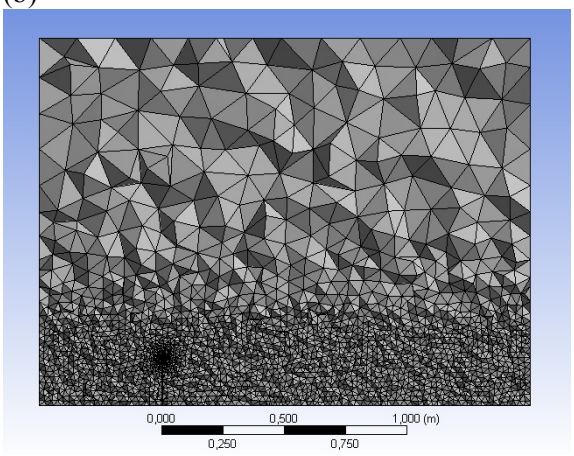

Fig.14. (a) The geometry of calculating field; (b) The grid

For accurate calculation grid has been constructed densely in the region of interest: around the exit of the pipe and across the path trajectory of emissions motion. Grid contains 568 486 three-dimensional cells. The numbers of elements are the same for the scale of 1:1000 and for 1:1. During the solution there was applied RANS (Reynolds-averaged Navier-Stokes equations). As in [5], it has been used RNG k-e turbulence model. Sizes were defined as follows as shown in Table 2.

Table 2. Geometry parameters

	Geometry dimensions [m]	**Stack dimensions [m]**	**Inlet dimensions [m]**	**Coordinates of stack [m]**
1:1000	X = 2.0 Y = 1.5 Z = 1.5	X= 0.0035 Y= 0.2 Z= 0.0035	X = 0.0035 Y = 0.0035	X = 0.5 Y = 0.0 Z= 0.75
1:1	X = 2000 Y = 1500 Z = 1500	X = 3.5 Y = 200 Z = 3.5	X =3.5 Y = 3.5	X = 500 Y = 0.0 Z = 750

As in the test problem, Species transport model was applied in order to calculate the movement of substances. It was assumed that there exist operating force of gravity and discharged substances do not react with air. The temperature was set as 3 00K (27C). Convergence criterion was set as $\varepsilon = 0.0001$. Such parameters as pressure, temperature, convergence criteria were specified analogically as in [5]. The Reynolds number is varied from 1017 to 2283, depending on t he wind speed and pollution density.

3.2 Boundary and initial conditions

Boundary conditions were set as the "*Velocity inlet"* for the enter of the wind pipe and the hole, "*Wall*" for pipe walls and the ground, "*Pressure Outlet*" for the outlet, "*Symmetry"* for the side walls and the top wall.

To validate the effect of the initial velocity profile it was done comparative analysis of the results for calculations with the constant velocity, independent of the height: $v_x = 5\,[m\ s^{-1}]$ and the velocity profile: $v_x = 5.0 \cdot (0.2371 \cdot \ln(Y + 0.00327) + 1.3571)\,[m\ s^{-1}]$.

The comparative analysis with [5] was carried out, in order to verify the correctness of the configurable parameters in ANSYS. For this purpose the motion of helium was considered in geometry of real scale 1:1. The velocity of helium was 0.5 m/s. Below in Figure 15 the results of foreign authors are shown.

In order to verify model in this case, the wind velocity of 5 m/s was chosen. Here, Figure 16 illustrates the results obtained in this work.

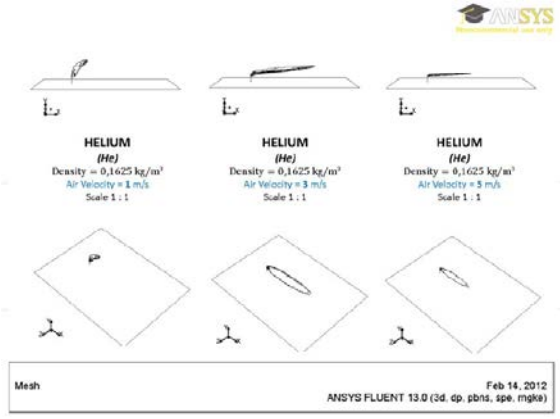

Fig.15. Results of the helium in [5] at different wind velocities: 1 m/s, 3 m/s and 5 m/s at 1:1 scale.

(a)

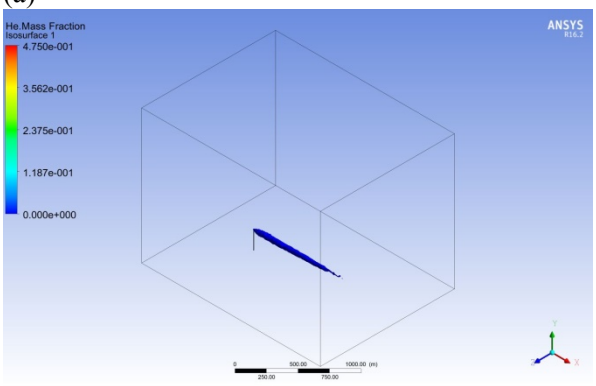

(b)

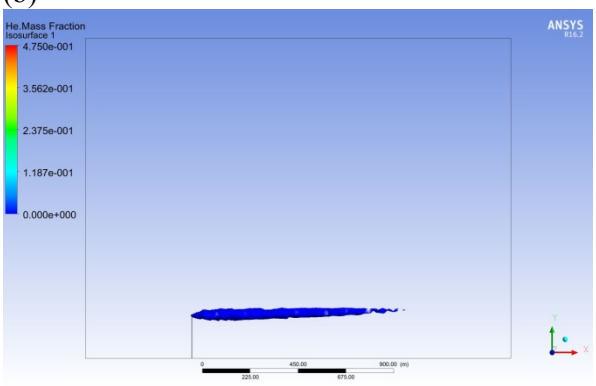

Fig.16. Gas pollutant plume motion analysis in 1:1 scale (contours of He concentration, $v_X = 5.0 \cdot \left(0.2371 \cdot \ln\left(Y + 0.00327\right) + 1.3571\right)\left[m\ s^{-1}\right]$): (a) XYZ , (b) XY plane

After checking the correctness of the chosen solution algorithm and configuration parameters, the different types of most common pollutants considered. In this case SO2, CO2 and SO were modeled.

The following Figures 17-19 show the resulting graphs of their spreading. The convergence criterion was set as 0.0001. Data visualized using Isosurface option, the maximum concentration was set as 0.00003.

a)

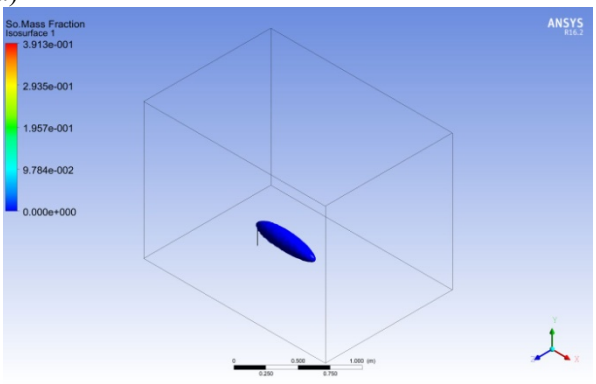

(b)

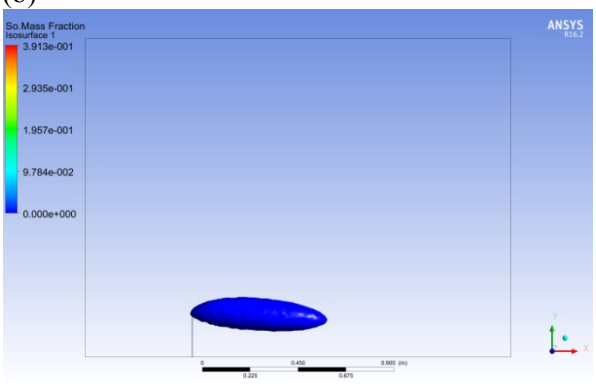

Fig.17. Gas pollutant plume motion analysis in 1:1000 scale (contours of SO concentration, $v_X = 5.0 \cdot \left(0.2371 \cdot \ln\left(Y + 0.00327\right) + 1.3571\right)\left[m\ s^{-1}\right]$): (a) XYZ , (b) XY plane

(a)

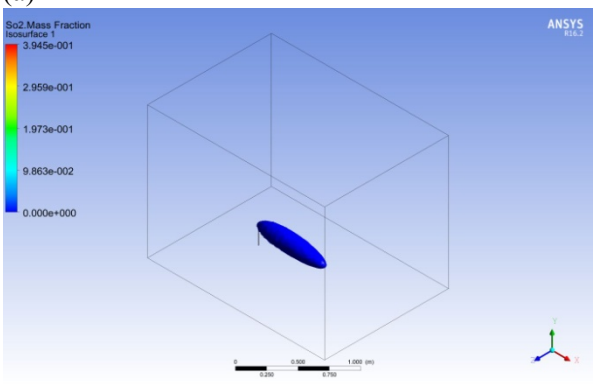

(b)

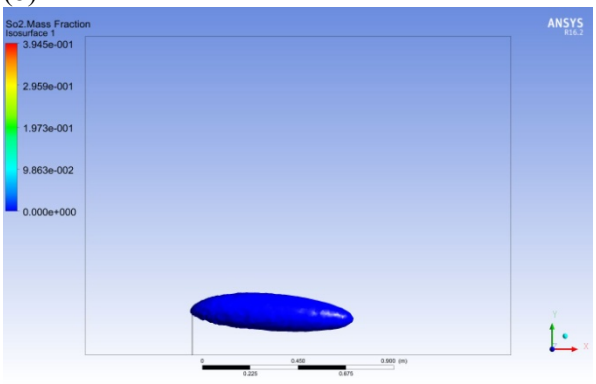

Fig.18. Gas pollutant plume motion analysis in 1:1000 scale (contours of SO2 concentration, $v_x = 5.0 \cdot \left(0.2371 \cdot \ln\left(Y + 0.00327\right) + 1.3571\right) [m\ s^{-1}]$): (a) XYZ , (b) XY plane

(a)

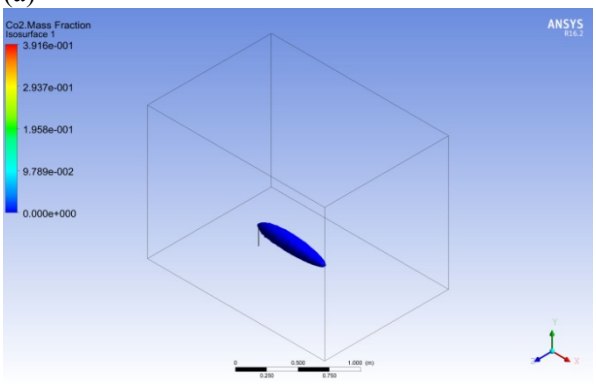

(b)

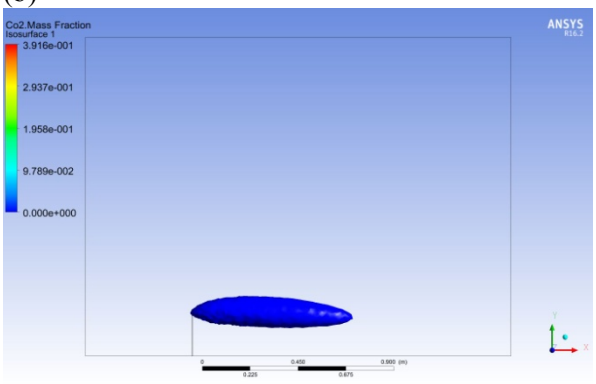

Fig.19. Gas pollutant plume motion analysis in 1:1000 scale (contours of CO2 concentration, $v_x = 5.0 \cdot \left(0.2371 \cdot \ln\left(Y + 0.00327\right) + 1.3571\right) [m\ s^{-1}]$): (a) XYZ , (b) XY plane

The following Figures 20-22 illustrate the profiles of pollution distribution from the stack hole at various distances from the chimney: 0.2 [m], 0.5[m], 1.0[m]. As the chimney located at the distance x=0.5 from the wind velocity inlet (see Table 2), the sections were taken at x=0.7, x=1.0, x=1.5 [m] from the wind inlet.

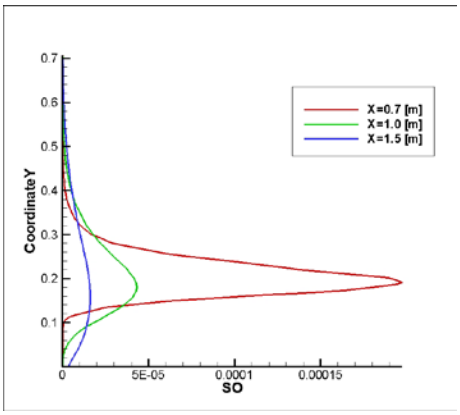

Fig.20. Profile of SO mass fraction.

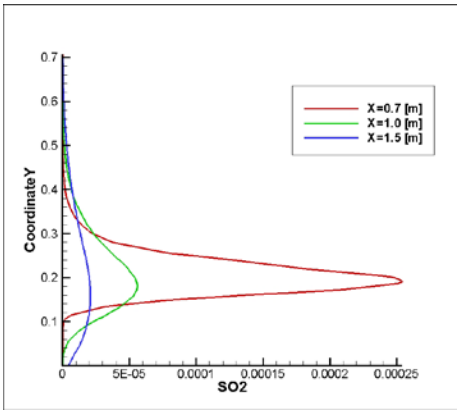

Fig.21. Profile of SO2 mass fraction.

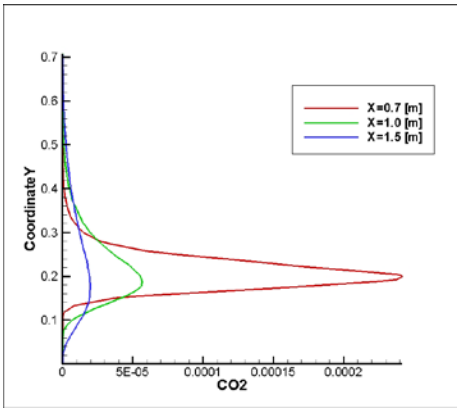

Fig.22. Profile of CO2 mass fraction.

Previous three-dimensional problem was modeled for scale 1:1000. Geometry settings can be found in Table 2. The following problem modeled in real physical scales. All other parameters remain the same.

The following Figures 23 - 25 show the results in the 1:1 scale for the SO, SO2, CO2 gases, respectively.

(a)

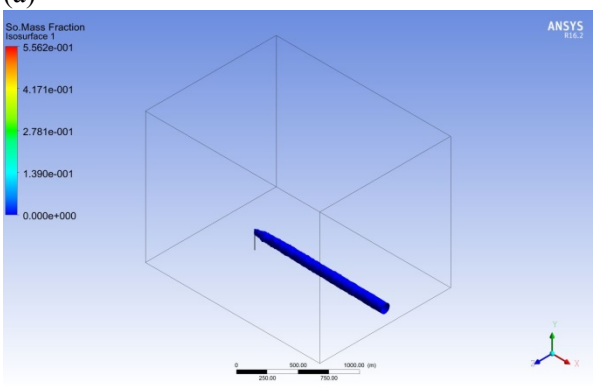

(b)

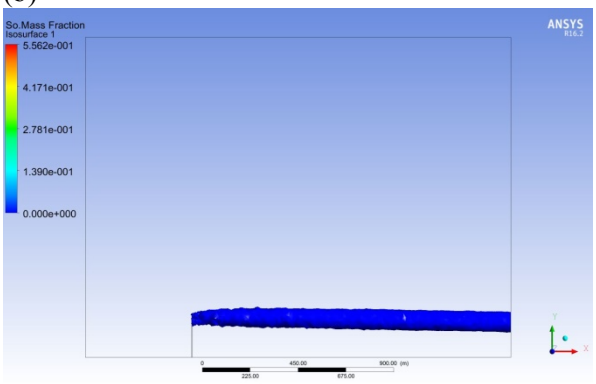

Fig.23. Gas pollutant plume motion analysis in 1:1 scale (contours of *SO* concentration): (a) XYZ , (b) XY plane

a)

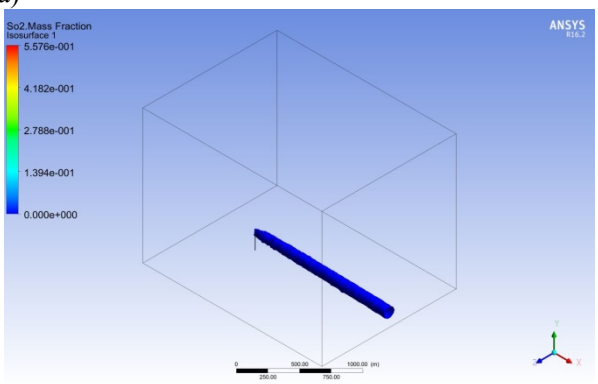

(b)

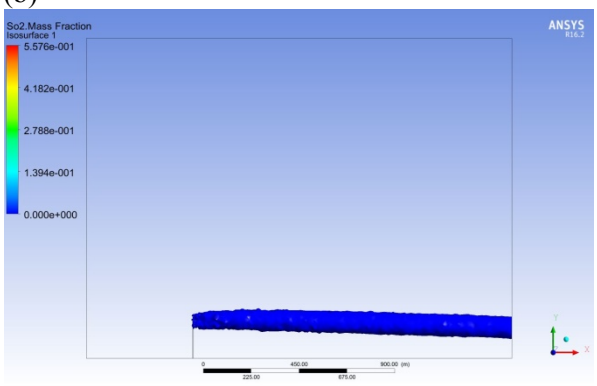

Fig.24. Gas pollutant plume motion analysis in 1:1 scale (contours of SO2 concentration): (a) XYZ , (b) XY plane

(a)

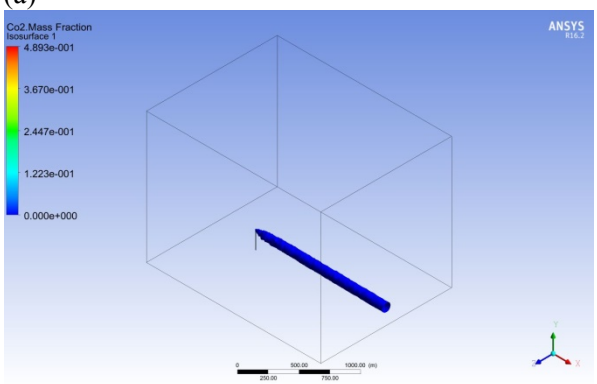

(b)

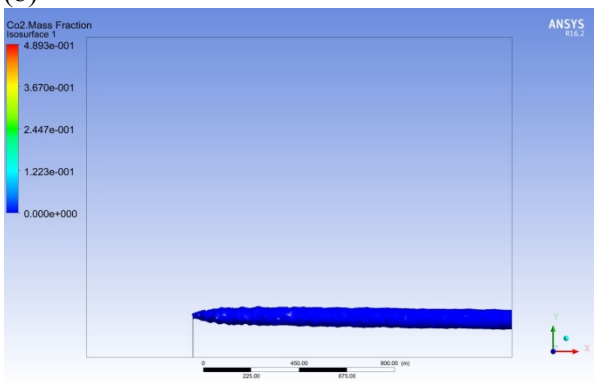

Fig.25. Gas pollutant plume motion analysis in 1:1 scale (contours of CO2 concentration): (a) XYZ , (b) XY plane

The following Figures 26-28 illustrate the profiles of pollution distribution from the stack hole at various distances: 200 [m], 500 [m], 1000 [m]. The chimney located at the distance x=500 [m] from the wind velocity inlet (see Table 2), that is why as in

the case of 1:1000 scale, the sections were taken at x=700, x=1000, x=1500 [m] from the wind inlet.

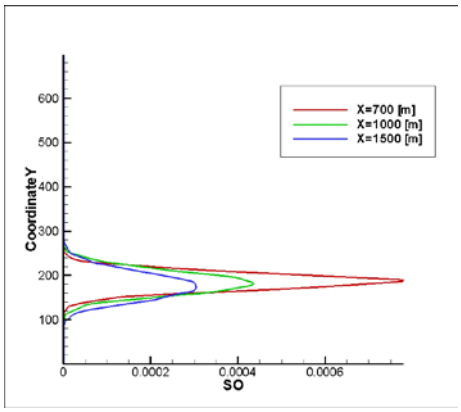

Fig.26. Profile of SO mass fraction.

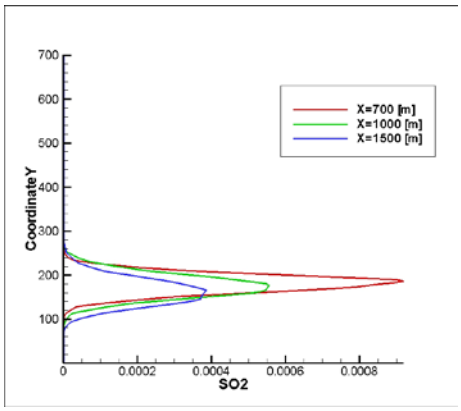

Fig.27. Profile of SO2 mass fraction.

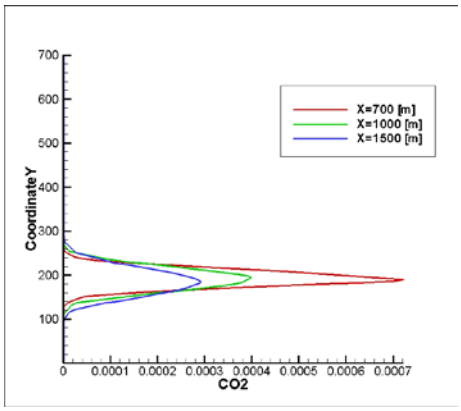

Fig.28. Profile of CO2 mass fraction.

Next, we consider the case of the presence of obstacles. In various cases, near from the thermal or nuclear power plants can be located buildings, mountains, towers, etc. That is why we have considered the building barriers. The distance from the pipe to the building is 1,1 km. The height of the building is 100 m. Its length and width are 10m.

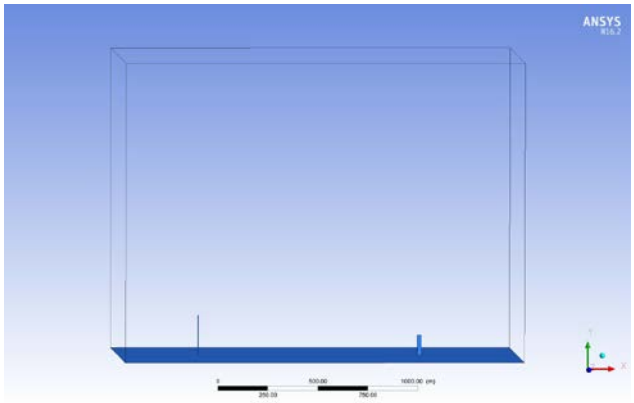

Fig.29. The geometry of calculating field with the obstacle.

(a)

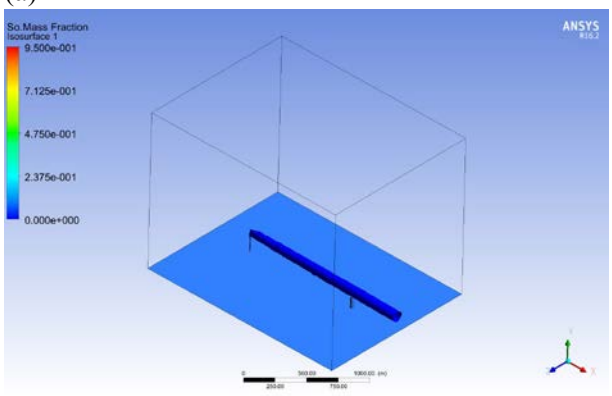

(b)

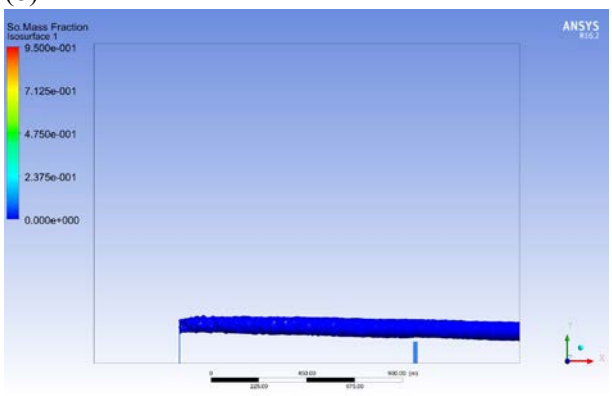

Fig.30. Gas pollutant plume motion analysis in 1:1 scale (contours of SO concentration), in the case with obstacle: (a) XYZ , (b) XY plane

The next figures illustrate the spreading of the SO, SO2, CO2 in the case with obstacle.

(a)

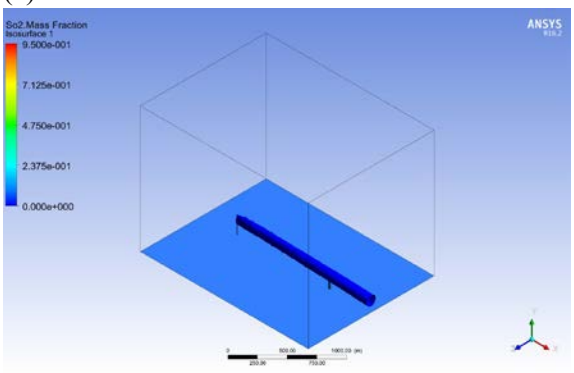

(b)

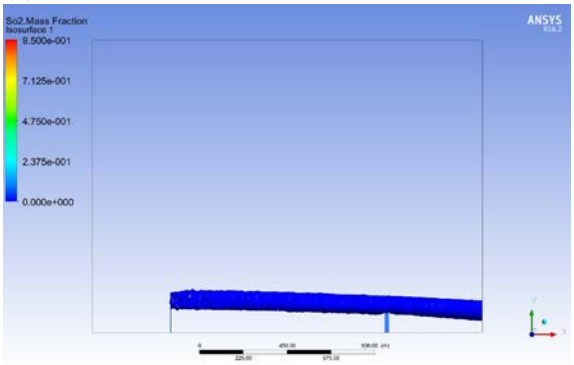

Fig.31. Gas pollutant plume motion analysis in 1:1 scale (contours of SO2 concentration), in the case with obstacle: (a) XYZ , (b) XY plane

(a)

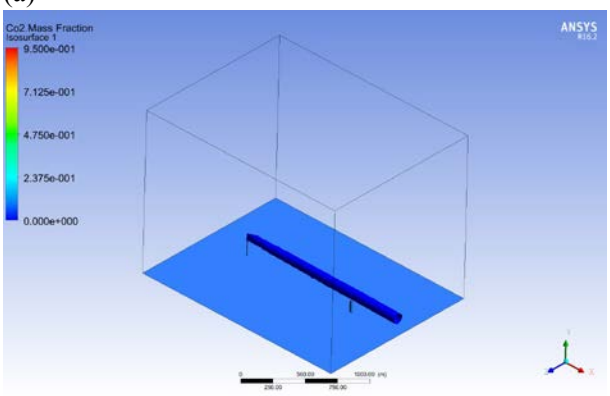

(b)

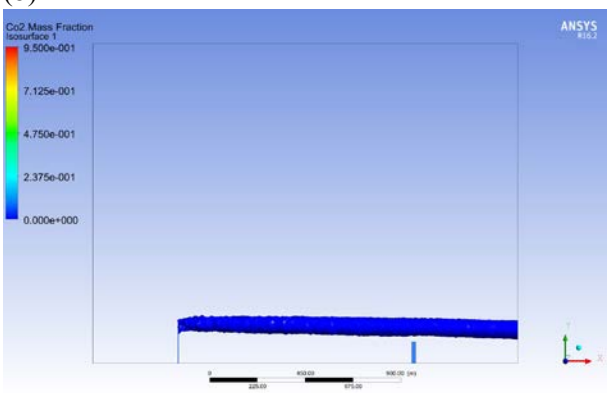

Fig.32. Gas pollutant plume motion analysis in 1:1 scale (contours of CO2 concentration), in the case with obstacle: (a) XYZ , (b) XY plane

The following figures show graphs of distribution of gases at the distances 1400, 1510 and 1600 [m].

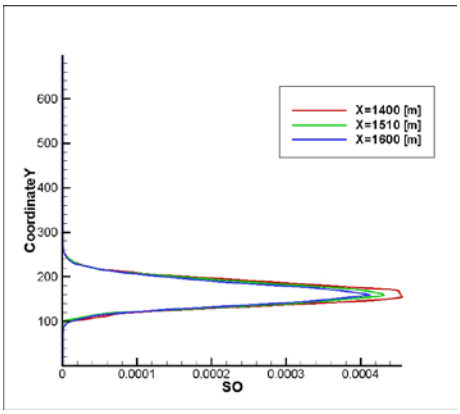

Fig.33. Profile of SO mass fraction in the case with obstacles.

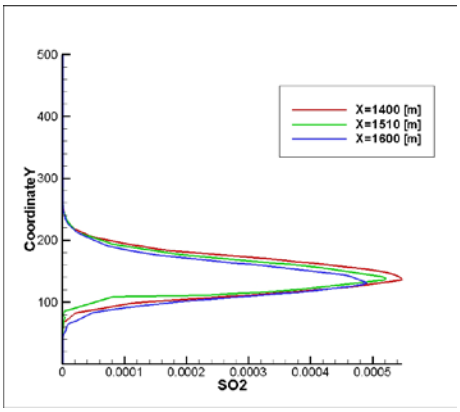

Fig.34. Profile of SO2 mass fraction in the case with obstacles.

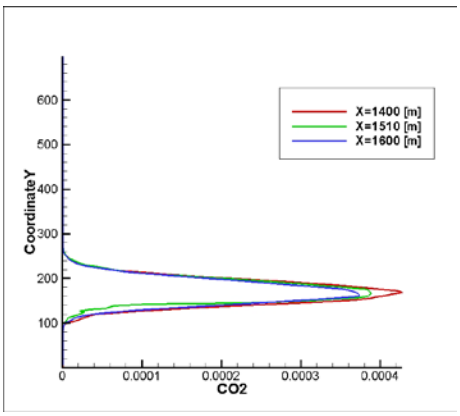

Fig.35. Profile of CO2 mass fraction in the case with obstacles.

Next, we considered the real physical model of the spread of contamination from Ekibastuz Thermal Power Plant 2, located in Ekibastuz. At this station there are existed two pipes, their heights are 300 and 330 m. The distance between the pipes is about 250 m. (Figure 36). Distance to nearby buildings is about 200 m. Diameter of pipe is 10 m.

Fig.36. Satellite image of Ekibastuz Thermal Power Plant 2 and the distance between the pipes (250 m).

(a)

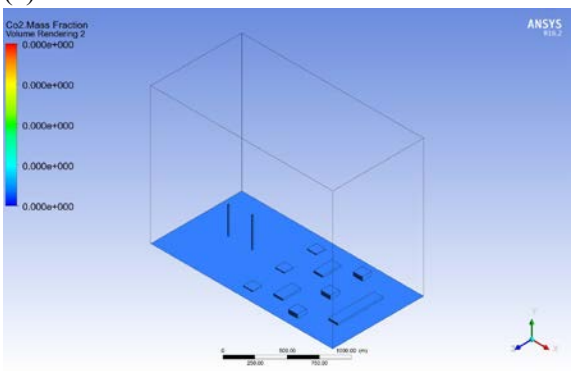

(b)

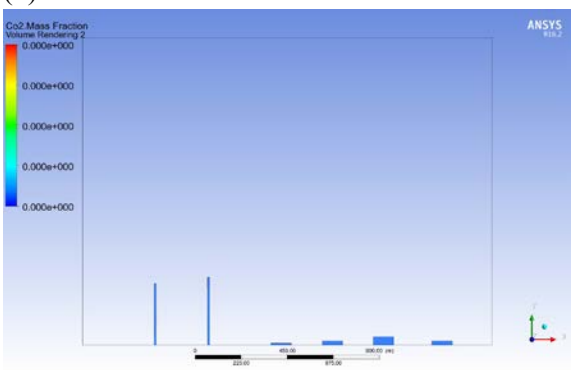

Fig.37. Geometry of the Ekibastuz Thermal Power Plant 2.

By using the real parameters, there was implemented the designing of power plant's geometry and the numerical simulation of pollution spreading.

At the following Figure there is illustrated the distribution of SO2.

(a)

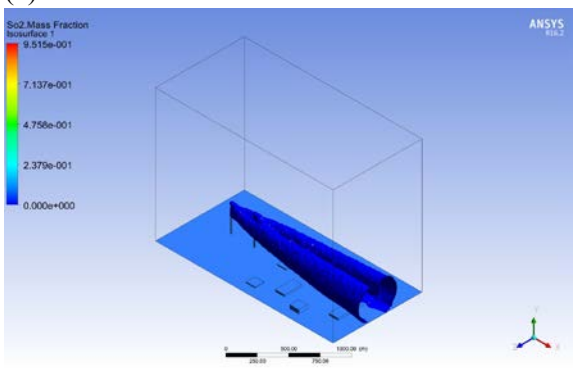

(b)

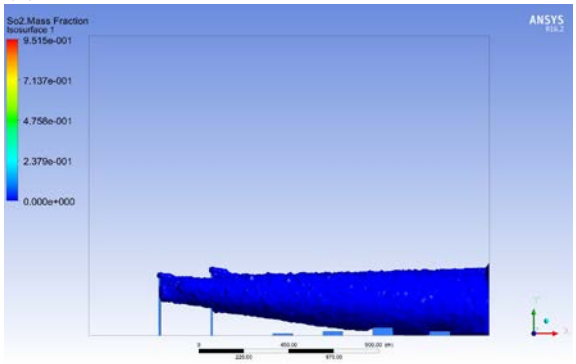

Fig.38. Gas pollutant plume motion analysis in 1:1 scale (contours of SO2 concentration), in the case with obstacle: (a) XYZ , (b) XY plane

4 Conclusion And Analysis Of Results

The aim of this work was to study and analysis of the propagation substances in the atmosphere with the influence of air velocity, density of ejected material, pipe dimensions and other atmospheric conditions. The solution of a simplified model problem allows to validate the correctness of the chosen mathematical model and numerical solution method, which subsequently can be used in the calculations of more complicated turbulent models. The motion of substance, which enters from the jet, flowing across the main crossflow was considered. Physical parameters such as d ensity, dynamic viscosity, hydraulic diameter and velocity, were selected so as to obtain a low Reynolds number for laminar flow. Due to the fact that in the calculation models of complex turbulent distribution of emissions from thermal and nuclear power plants there are considered concentration and mass ratio of different chemicals, it is necessary to account the possibility of calculating the concentration in the mathematical models. Since the emission elements under the influence of chemical and physical parameters are mixed to form new components, into

the models and numerical algorithms there was included the possibility of calculating the chemical reaction. Obtained results showed that the exponent degree variation in the velocity profile has significant influence on the flow, but setting the velocity as t he constant gives a l arge error in calculation. Analysis showed that the airflow rate significantly affects the character and range of motion of the substances dissemination. After the solving of two-dimensional problem, there was implemented the three-dimensional numerical simulation. There were considered various cases: the distribution motion without any obstacles, with obstacles and in real physical scale, taking from the Ekibastuz Thermal Power Plant 2. This study provides a preliminary assessment of the spread for harmful substances in the atmosphere, taking into account physical, climatic and meteorological factors. Geometric parameters of the plants (height and width of the pipe) are also taken into account.

This method of research allows finding a distance of harmful substances distribution in the air that will help to simulate optimal location of thermal and nuclear power plants with respect to human settlements in advance. This minimized the damage caused by emissions to humans, flora and fauna. In this work we were considered the most common emissions (SO2, CO2, SO), coming from thermal power plants and nuclear power plants and causing the greatest harm to the environment. Constructed condensed grid will minimize calculations and focus on areas of interest to us.

References:

[1] *Ekologicheskiy kodeks Respubliki Kazahstan (s izmeneniyami i dopolneniyami po sostojaniyu na 11.04.2014 g.)*.

[2] Ryzhkin V. Ya. *Teplovye elektricheskie stancii*, / red V.Ya. Girshfelda .- M: Energoatomizdat.- 1987 g.- 321 s.

[3] Dukenbaev K. *Energetika Kazahstana. Tehnicheskiy aspekt*, - Almaty, 2001.-312 s.

[4] U.S. Environmental Protection Agency, Clean Air Markets Division: https://ampd.epa.gov/ampd/

[5] Zavila O. Physical Modeling of Gas Pollutant Motion in the Atmosphere, Advances in Modeling of Fluid Dynamics, Dr. Chaoqun Liu (Ed.), InTech, 2012, DOI: 10.5772/48405.

[6] Goyal P., Kumar A. Mathematical Modeling of Air Pollutants: An Application to Indian Urban City, Air Quality-Models and Applications, Prof. Dragana Popovic (Ed.), InTech, 2011, DOI: 10.5772/16840.

[7] Kozic, M. S. A numerical study for the assessment of pollutant dispersion from kostolac b pow er plant to viminacium for different atmospheric conditions // THERMAL SCIENCE, Vol. 19, No. 2.-2015.- pp. 425-434.

[8] Falconi C. J., Denev J. A., Frohlich J. and Bockhorn H. A test case for microreactor flows - a two-dimensional jet in crossflow with chemical reaction, Internal Report, available at: http://www.ict.uni-karlsruhe.de/index.pl/themen/dns/index.html: "2d test case for microreactor flows. Internal report. 2007 July 20, 2007.

[9] Schonauer, W., Adolph, T. FDEM: The Evolution and Application of the Finite Difference Element Method (FDEM) Program Package for the Solution of Partial Differential Equations, Abschlussbericht des Verbundprojekts FDEM, UniversitËat Karlsruhe.- 2005.- available at http://www.rz.uni-karlsruhe.de/rz/docs/FDEM/Literatur/fdem.pdf

[10] Margason, R. J. 1993 F ifty years of jet in crossflow research. In AGARD Symp. on a Jet in Cross Flow, Winchester, UK. AGARD CP 534.

[11] Kamotani, Y. & Greber, I. 1972 E xperiments on turbulent jet in a crossflow. AIAA J. 10, 1425–1429.

[12] Fearn, R. L. & Weston, R. P. 1974 Vorticity associated with a jet in crossflow. AIAA J. 12, 1666–1671.

[13] Andreopoulos, J. & Rodi, W. 1984 Experimental investigation of jets in a crossflow. J. Fluid Mech. 138, 93–127.

[14] Krothapalli, A., Lourenco, L. & Buchlin, J. M. 1990 Separated flow upstream of a jet in a crossflow. AIAA J. 28, 414–420.

[15] Fric, T. F. & Roshko, A. 1994 Vortical structure in the wake of a transverse jet. J. Fluid Mech. 279, 1–47.

[16] Kelso, R. M., Lim, T. T. & Perry, A. E. 1996 An experimental study of round jets in cross-flow. J. Fluid Mech. 306, 111–144.

[17] Smith, S. H. & Mungal, M. G. 1998 M ixing, structure and scaling of the jet in crossflow. J. Fluid Mech. 357, 83–122.

[18] Su, L. K. & Mungal, M. G. 2004 Simultaneous measurement of scalar and velocity field evolution in turbulent crossflowing jets J. Fluid Mech. 513, 1–45.

[19] Shan, J. W. & Dimotakis, P. E. 2006 Reynolds-number effects and anisotropy in transverse-jet mixing. J. Fluid. Mech. 566, 47–96.

[20] Broadwell, J. E. & Breidenthal, R. E. 1984 Structure and mixing of a transverse jet in incompressible flow. J. Fluid Mech. 148, 405–412.

[21] Karagozian, A. R. 1986 A n analytical model for the vorticity associated with a transverse jet. AIAA J. 24, 429–436.

[22] Hasselbrink, E. F. & Mungal, M. G. 2001 Transverse jets and jet flames. Part 1. Scaling laws for strong transverse jets. J. Fluid Mech. 443, 1–25.

[23] Muppidi, S. & Mahesh, K. 2005 Study of trajectories of jets in crossflow using direct numerical simulations. J. Fluid. Mech. 530, 81–100.

[24] Muppidi, S. & Mahesh, K. 2008 Direct numerical simulation of passive scalar transport in transverse jets. J. Fluid Mech., 598, pp. 335–360.

[25] Chochua, G., Shyy, W., Thakur, S., Brankovic, A., Lienau, K., Porter, L. & Lischinsky, D. 2000 A computational and experimental investigation of turbulent jet and crossflow interaction. Numer. Heat Transfer A 38, 557–572.

[26] Acharya, S., Tyagi, M. & Hoda, A. 2001 Flow and heat transfer predictions for film-cooling. Ann. NY Acad. Sci. 934, 110–125.

[27] Yuan, L. L., Street, R. L. & Ferziger, J. H. 1999 Large-eddy simulations of a round jet in crossflow. J. Fluid Mech. 379, 71–104.

[28] Schluter, J. U. & Schonfeld, T. 2000 LES of jets in crossflow and its application to a gas turbine burner. Flow Turbulence Combust. 65, 177–203.

[29] Chai, X., Iyer, P. S.,Mahesh, K. Numerical study of high speed jets in crossflow // Journal of Fluid Mechanics, Volume 785.- 2015. - 152-188 pp.

[30] Muppidi, S. & Mahesh, K. 2007 Direct numerical simulation of round turbulent jets in crossflow. J. Fluid. Mech. 574, 59–84.

[31] D. Livescu, F. A. Jaberi and C. K. Madnia. Passive-scalar wake behind a line source in grid turbulence. Journal of Fluid Mechanics. Volume 416, 2000, pp 117- 149.

[32] R. Camussi, G. Guj and A. Stella. Experimental study of a jet in a crossflow at very low Reynolds number. Journal of Fluid Mechanics. Volume 454, 2002, pp 113- 144.

[33] Chung T. J. Computational Fluid Dynamics. Cambridge University Press, 2002 - p. 1012.

[34] Ferziger J. H., Peric M. Computational Methods for Fluid Dynamics. Springer; 3rd edition, 2013, -p. 426

[35] Issakhov A. Large eddy simulation of turbulent mixing by using 3D decomposition method. Issue 4 / / J. Phys.: Conf. Ser. 318. pp. 1282-1288. -2011. doi:10.1088/1742-6596/318/4/042051.

[36] Issakhov A. Mathematical modeling of the discharged heat water effect on t he aquatic environment from thermal power plant // International Journal of Nonlinear Science and Numerical Simulation, 16(5). -2015, -229-238 pp., doi:10.1515/ijnsns-2015-0047.

[37] Issakhov A. Mathematical modeling of the discharged heat water effect on the aquatic environment from thermal power plant under various operational capacities // Applied Mathematical Modelling (2015), Volume 40, Issue 2, -2016, - 1082-1096 pp. http://dx.doi.org/10.1016/j.apm.2015.06.024.